

(This is a sample cover image for this issue. The actual cover is not yet available at this time.)

This article appeared in a journal published by Elsevier. The attached copy is furnished to the author for internal non-commercial research and education use, including for instruction at the authors institution and sharing with colleagues.

Other uses, including reproduction and distribution, or selling or licensing copies, or posting to personal, institutional or third party websites are prohibited.

In most cases authors are permitted to post their version of the article (e.g. in Word or Tex form) to their personal website or institutional repository. Authors requiring further information regarding Elsevier's archiving and manuscript policies are encouraged to visit:

<http://www.elsevier.com/copyright>



Contents lists available at SciVerse ScienceDirect

NeuroImage

journal homepage: www.elsevier.com/locate/ynimg

Changes in the brain intrinsic organization in both on-task state and post-task resting state

Zhijiang Wang^{a,b}, Jiming Liu^{a,b,c}, Ning Zhong^{a,b,d,*}, Yulin Qin^{a,b,e}, Haiyan Zhou^{a,b}, Kuncheng Li^{f,b,**}

^a International WIC Institute, Beijing University of Technology, China

^b Beijing Key Laboratory of MRI and Brain Informatics, China

^c Department of Computer Science, Hong Kong Baptist University, Hong Kong

^d Department of Life Science and Informatics, Maebashi Institute of Technology, Japan

^e Department of Psychology, Carnegie Mellon University, USA

^f Department of Radiology, Xuanwu Hospital, Capital Medical University, China

ARTICLE INFO

Article history:

Accepted 27 April 2012

Available online 5 May 2012

Keywords:

Modulation

Topology

Small world

Default mode network

Task-driven states

ABSTRACT

The dynamic and robust characteristics of intrinsic functional connectivity of coherent spontaneous activity are critical for the brain functional stability and flexibility. Studies have demonstrated modulation of intrinsic connectivity within local spatial patterns during or after task performance, such as the default mode network (DMN) and task-specific networks. Moreover, recent studies have compared the global spatial pattern in different tasks or over time. However, it is still unclear how the large-scale intrinsic connectivity varies during and after a task. To better understand this issue, we conducted a functional MRI experiment over three sequential periods: an active semantic-matching task period and two rest periods, before and after the task respectively (namely, on-task state and pre-/post-task resting states), to detect task-driven effect on the dynamic large-scale intrinsic organization in both on-task state and post-task resting state. Three hierarchical levels were investigated, including (a) the whole brain small-world topology, (b) the whole pairwise functional connectivity patterns both within the DMN and between the DMN and other regions (i.e., the global/full DMN topography), and (c) the DMN nodal graph properties. The major findings are: (1) The large-scale small-world configuration of brain functional organization is robust, regardless of the behavioral state changing, while it varies adaptively with significantly higher local efficiency and lower global efficiency during the on-task state ($P < 0.05$, Monte-Carlo corrected); (2) The DMN may be essentially engaged during both task and post-task processes with adaptively varied spatial patterns and nodal graph properties. The present study provides further insights into the robustness and plasticity of the brain intrinsic organization over states, which may be the basis of memory and learning in the brain.

© 2012 Elsevier Inc. All rights reserved.

Introduction

Spontaneous brain activity, utilizing the majority of brain energy in specific organizations over different states or time (Raichle and Mintun, 2006), may substantially account for the dynamic, robust intrinsic functional architecture of the brain (for a review, see Fox and Raichle, 2007). This activity is also related to the establishment of early cortical patterns (Price et al., 2006; Sur and Leamey, 2001) and the development of intrinsic functional networks over ages (Fair et al., 2008, 2009). From an evolutionary perspective at a much larger temporal scale, the brain organization has evolved to a marvelous highly-complex system, with supporting dynamic and effective integration of specialized local information processing (Sporns and Zwi, 2004) and a

broad flexibility of cognitive processes (Sporns et al., 2004). So, it is important to investigate the brain intrinsic organization of coherent spontaneous activity for understanding how the brain works.

By functional connectivity (Friston et al., 1993), studies have identified many intrinsic spatial patterns in coherent low-frequency blood oxygen level dependent (BOLD) fluctuations of functional MRI (fMRI) during a continuous resting state. For instance, local spatial patterns have been identified among anatomically separated regions in neuro-anatomical systems, including the motor (Biswal et al., 1995; Lowe et al., 1998), auditory (Cordes et al., 2001), visual (Lowe et al., 1998), language (Hampson et al., 2002), attention (Fox et al., 2006) and default-mode systems (the default mode network, DMN) (Fox et al., 2005; Greicius et al., 2003). The local spatial patterns can provide insights into the intrinsic functional architecture of the human brain (Fox and Raichle, 2007). On the other hand, for the global spatial pattern over the whole brain, topological properties such as the small-world characteristics (high clustering coefficient and short characteristic path distance) and power-law (or truncated power-law) degree distribution have been demonstrated (for reviews, see Bassett and Bullmore, 2006;

* Correspondence to: N. Zhong, International WIC Institute, Beijing University of Technology, China, and the Department of Life Science and Informatics, Maebashi Institute of Technology, Maebashi-City, 371-0816, Japan. Fax: +86 10 67396667.

** Correspondence to: K. Li, Department of Radiology, Xuanwu Hospital, Capital Medical University, China.

E-mail addresses: zhong@maebashi-it.ac.jp (N. Zhong), lkc1955@gmail.com (K. Li).

Bullmore and Sporns, 2009; Sporns et al., 2004) in both large-scale functional (Achard et al., 2006; Eguíluz et al., 2005; Salvador et al., 2005a, 2005b; Van den Heuvel et al., 2008) and structural (Hagmann et al., 2007; He et al., 2007; Iturria-Medina et al., 2008) networks. The small-world organization can support both functional segregation and integration (for reviews, see Bassett and Bullmore, 2006; Sporns and Zwi, 2004; Sporns et al., 2004), which are two fundamental organizational principles of the cerebral cortex (Friston, 2002; Tononi et al., 1998; Zeki and Shipp, 1988). It can also facilitate rapid adaptive reconfiguration of neuronal assemblies in support of the cognitive state changing (Bassett and Bullmore, 2006).

Studies have also demonstrated that the intrinsic spatial patterns of coherent spontaneous activity could be modulated during a task (Bianciardi et al., 2009; Calhoun et al., 2008; Fransson, 2006; Friston and Büchel, 2000; Hampson et al., 2002; Jiang et al., 2004; Liu et al., 1999; Lowe et al., 2000), or after task performance (Hasson et al., 2009; Lewis et al., 2009; Peltier et al., 2005; Tambini et al., 2010; Waites et al., 2005). We suggest that both on-task and subsequent resting (post-task) states could be called “task-driven” states. Of all the local intrinsic spatial patterns, the DMN is uniquely a set of brain regions remaining more active at rest than during task performance in an organized fashion (Fox et al., 2005; Greicius et al., 2003), and is thought to mediate processes that are important for the resting state (Raichle et al., 2001). Several local spatial patterns within the DMN have been demonstrated to be changed in both task-driven states, including an on-task state (Fransson, 2006) and a post-task resting state (Hasson et al., 2009; Tambini et al., 2010; Waites et al., 2005). At a larger temporal scale, studies have also suggested that intrinsic brain functional networks would be developing over ages in specific ways (Fair et al., 2008, 2009). By contrast, some other studies reported no significant change in a local DMN spatial pattern based on a seed region of posterior cingulate cortex (PCC) during task performance (Greicius et al., 2003; Hampson et al., 2006), and nor in a task-specific network after task performance (Albert et al., 2009).

On the other hand, for the variability of the global spatial pattern across states, a pioneer work by Bassett et al. (2006) using magnetoencephalograph (MEG) suggests that small-world properties are not sensitive to a visually cued finger tapping task. However, there are two limitations of that study: (1) they did not design sequential sessions of task and rest; (2) MEG sensors may be problematic in network node definitions, because the sensors may detect spatially overlapping signals (Ioannides, 2007; Rubinov and Sporns, 2010). There are other different studies investigating changes in large-scale brain network topology over time during learning (Bassett et al., 2011), or with respect to different working memory tasks (Ginestet and Simmons, 2011), or over ages at a large temporal scale (Fair et al., 2009; Meunier et al., 2009; Wang et al., 2010). It appears that the dynamic characteristics of intrinsic functional connectivity of coherent spontaneous activity are critical for the brain functional stability and flexibility. Hence, it is necessary to investigate the robustness and plasticity of the large-scale intrinsic organization of coherent spontaneous activity in terms of the “small-world” and the DMN topological properties together in both task-driven states.

The present study focused on a sequential procedure of pre-task resting, on-task and post-task resting states by fMRI, and investigated task-driven effect on the dynamic large-scale intrinsic functional organization in both on-task state and post-task resting state (see Fig. 1A). Three hierarchical levels of topologies were investigated, including (a) the whole brain small-world topology, (b) the whole pairwise functional connectivity patterns both within the DMN and between the DMN and other regions (i.e., the global/full DMN topography), and (c) the DMN nodal graph properties (see Fig. 1B). Small-world analysis could macroscopically characterize the balanced coordination between the local specialization and global integration of parallel information processing (functional segregation and integration). The DMN topological

analysis could provide insights into lower-level dynamic topological properties in the large-scale intrinsic organization. Thus, the specific question examined in this study is what topological changes would occur in the large-scale intrinsic organization when the brain evolves from a pre-task-resting state to both task-driven states, in terms of (1) the small-world configuration and (2) the global DMN topography and nodal properties.

To answer this question, we conducted an fMRI experiment that recorded BOLD signals over three sequential periods: an active semantic-matching task period and two rest periods, before and after the task respectively. Under the three states, we constructed three groups of brain functional networks for each subject using a prior anatomical automatic labelling (AAL) atlas (see Table 1, 45 for each cerebral hemisphere, Tzourio-Mazoyer et al., 2002) in the low-frequency BOLD signals (0.01–0.08 Hz). Finally, the three-level topologies in terms of the small-world configuration, the global DMN topography and its nodal properties were investigated across states, and their differences between the task-driven states and pre-task resting state were further statistically evaluated. This three-level topological analysis could provide further insights into the robustness and plasticity of the intrinsic organization during or after a task.

Material and methods

Subjects

Fifteen healthy subjects (7 males, 8 females; 23.8 ± 0.7 years old) from Beijing University of Technology participated in the study. All the subjects were right-handed and reported with no history of neurological or psychiatric disorders. Written informed consent was obtained from each subject. All the subjects were scanned not only during a semantic-matching task (Zhou et al., 2010) but also during rests before and after the task. During the rest scans, subjects were instructed to relax with their eyes closed and move as little as possible.

Data acquisitions

Participants were scanned on 3.0 Tesla Siemens MRI scanner with the parameters: repetition time/echo time = 2000/31 ms, thickness/gap = 3.2/0 mm, matrix = 64×64 , axial slices number = 32 and field of view = 200×200 mm². The whole brain functional images using an echo planar imaging (EPI) sequence were acquired over all sessions. The whole scans contained five sessions with 8 min and 14 s (244 volumes) for each one, in which the first and last sessions were at rest while the intermediate three sessions were involved in a word-picture matching task (Zhou et al., 2010). During the task trials, a word was first presented then followed by a picture, and subjects were instructed to judge whether the picture matched the word or not (Zhou et al., 2010). Hence, the five sessions could be divided into three sequential behavioral states: pre-task resting state (the first session), on-task state (the intermediate three sessions), and post-task resting state (the last session). To allow for magnetization equilibrium, subjects' adaptation to the circumstances and separation between two adjacent sessions, the first 4 volumes of EPI sequence of each session for each subject were discarded, with leaving 240 volumes for each session available for further processing.

Data preprocessing

Images were first preprocessed using the software package of statistical parametric mapping (SPM5, <http://www.fil.ion.ucl.ac.uk/spm>) over sessions, respectively. First, all the images were corrected for the acquisition time delay by slice timing, and then were realigned to the first volume for head-motion correction in each session. Next, all the images were spatially normalized to the Montreal Neurological Institute (MNI) EPI template and resampled to 3 mm cubic voxels, without smoothing.

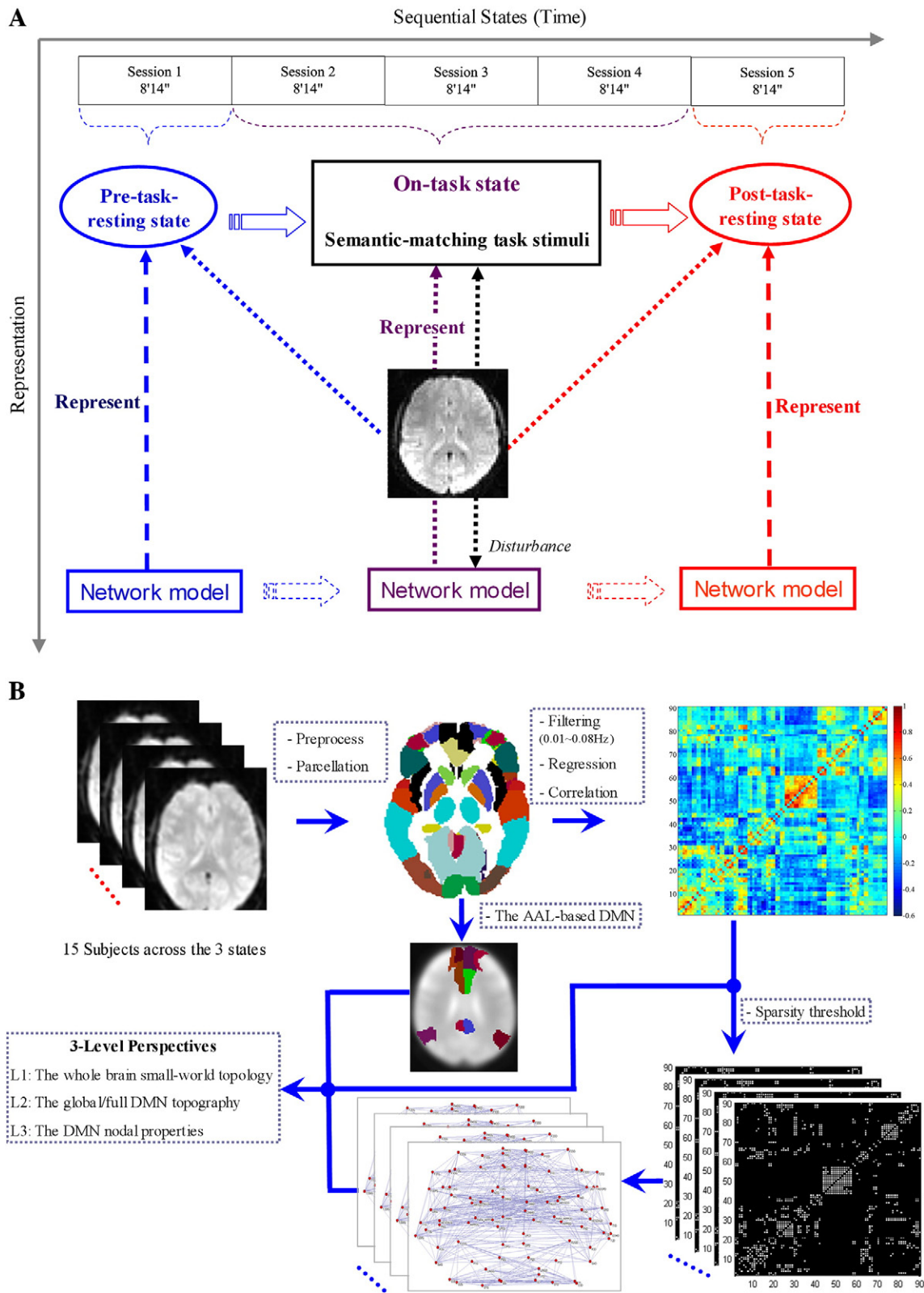


Fig. 1. Overview of the investigation. **A:** The whole scan included 5 sessions \times 8'14", in which the first and last sessions were at rest while the intermediate three sessions consisted of alternative trials of task (word-picture matching) and fixation (baseline). Hence, the five sessions could determine three sequential behavioral states: pre-task resting state (the first session), on-task state (the intermediate three sessions), and post-task resting state (the last session). The present study aimed to reveal task-driven effect on the dynamic large-scale intrinsic functional organization in both on-task state and post-task resting state through three levels; **B:** General analysis process. Three-level topologies were investigated, including (a) the whole brain small-world topology, (b) the global/full DMN topography (i.e., connectivity patterns both within the DMN and between the DMN and other regions), and (c) the DMN nodal graph properties.

Table 1
Regions of interest in the AAL-atlas.

Partitions	Regions of interest	
Frontal	Frontal_Sup_L/R	
	Frontal_Sup_Orb_L/R	
	Frontal_Mid_L/R	
	Frontal_Mid_Orb_L/R	
	Frontal_Inf_Oper_L/R	
	Frontal_Inf_Tri_L/R	
	Frontal_Inf_Orb_L/R	
	Frontal_Sup_Medial_L/R	
	Frontal_Med_Orb_L/R	
	Rectus_L/R	
	Parietal	Precentral_L/R
		Supp_Motor_Area_L/R
		Postcentral_L/R
		Parietal_Sup_L/R
Parietal_Inf_L/R		
SupraMarginal_L/R		
Angular_L/R		
Precuneus_L/R		
Occipital	Paracentral_Lobule_L/R	
	Calcarine_L/R	
	Cuneus_L/R	
	Lingual_L/R	
	Occipital_Sup_L/R	
	Occipital_Mid_L/R	
	Occipital_Inf_L/R	
Temporal	Fusiform_L/R	
	Rolandic_Oper_L/R	
	Insula_L/R	
	Hippocampus_L/R	
	ParaHippocampal_L/R	
	Amygdala_L/R	
	Heschl_L/R	
	Temporal_Sup_L/R	
	Temporal_Pole_Sup_L/R	
	Temporal_Mid_L/R	
	Temporal_Pole_Mid_L/R	
	Temporal_Inf_L/R	
Cingulum	Cingulum_Ant_L/R	
	Cingulum_Mid_L/R	
	Cingulum_Post_L/R	
Subcortical	Olfactory_L/R	
	Caudate_L/R	
	Putamen_L/R	
	Pallidum_L/R	
	Thalamus_L/R	

After those, each brain was then parcelled into 90 cortical and sub-cortical regions using the AAL-atlas (see Table 1). Then, each regional (90 regions of interest (ROIs)) time series were acquired by averaging the time series over all voxels within each ROI, and filtered into the frequency range of 0.01–0.08 Hz to reduce the effects of low-frequency drift and high-frequency noise, followed by a multiple linear regression analysis to remove several sources of spurious variances from the estimated head-motion profiles (six parameters obtained from head-motion correction) and global brain signal (Fox et al., 2005). The residual of the linear regression was considered the neuronal-induced signal of each corresponding region.

Construction of large-scale brain functional networks

Large-scale brain functional networks were constructed as the global spatial patterns of coherent brain BOLD activity over the three sequential states. The 90 ROIs from the AAL-atlas were defined as nodes. Edges were determined by whether the strength of functional connectivity between any pair of ROIs exceeded a threshold. To measure the functional connectivity, we calculated Pearson correlation coefficients of time series (BOLD signals) between any pair of brain regions, followed by a Fisher's *r*-to-*z* transformation (Jenkinson and Watts, 1968) to improve the normality of the correlation coefficients. Then, a temporal correlation matrix (90×90) was obtained for each subject during

each session. For the on-task state (the intermediate three sessions), the correlation matrices (after the Fisher's *r*-to-*z* transformation) were averaged over the three sessions for each subject. Thus, three groups of correlation matrices were acquired corresponding to the three sequential behavioral states, respectively. Finally, each correlation matrix was thresholded by a flexible threshold value T (≥ 0) into a binary matrix whose element was 1 if the corresponding correlation exceeded T and 0 otherwise. These processes resulted in three groups of binary undirected graphs underlying the large-scale brain functional organization.

Extraction of the default mode network and its spatial topography

In the present work, the DMN regions were determined from the AAL-atlas primarily according to the coordinates of the peak foci of all the “task-negative” regions (Fox et al., 2005). The ROIs in the AAL-atlas which covered the coordinates or the most adjacent ones were selected. Two coordinates (−3, 39, −2) and (1, 54, 21) were close to the inter-hemisphere locations between the left and right homogeneous regions, so the corresponding bilateral AAL-atlas regions were also selected. Last, the peak coordinate (−2, −36, 37) is near the boundary between cingulum_Mid_L and cingulum_Post_L, but the great part of the left PCC in Fox et al. (2005) is involved in cingulum_Post_L, so we selected cingulum_Post_L as the corresponding left PCC. Totally fourteen regions were selected as the AAL-based DMN components (see Table 2 and Fig. 1B). Finally, the global DMN topography were extracted from the 90×90 global correlation topography (after the Fisher's *r*-to-*z* transformation), which includes the pairwise functional connectivity patterns both within the fourteen DMN regions (the intra-DMN functional connectivity) and between them and non-DMN regions (the extra-DMN functional connectivity).

Small-world efficiencies

Global and local network efficiencies (E_{global} and E_{local} , see the equations below) are firstly defined by Latora and Marchiori to measure the capability of parallel information transfer in global and local

Table 2
Default mode/task-negative regions (Fox et al., 2005) defined in the AAL-atlas.

Regions of interest in the AAL	Talairach coordinates (x, y, z) in Fox et al. (2005)	Common names used in Fox et al. (2005)
Frontal_Sup_L	(−14, 38, 52)*	Superior frontal
Frontal_Sup_R	(17, 37, 52)	
Frontal_Sup_Medial_L	(1, 54, 21)	Medial prefrontal cortex (MPF)
Frontal_Sup_Medial_R		
Cingulum_Ant_L	(−3, 39, −2)	Medial prefrontal cortex (MPF)
Cingulum_Ant_R		
Cingulum_Post_L	(−2, −36, 37)*	Posterior cingulate gyrus / precuneus (PCC)
Cingulum_Post_R	(3, −51, 8)*	Retro-splenial
ParaHippocampal_L	(−22, −26, −16)	Parahippocampal gyrus
ParaHippocampal_R	(25, −26, −14)	
Angular_L	(−47, −67, 36)	Lateral parietal cortex (LP)
Angular_R	(53, −67, 36)	
Temporal_Mid_R	(65, −17, −15)	Inferior temporal
Temporal_Inf_L	(−61, −33, −15)	

Column 2 is the coordinates of the peak foci of all the “task-negative” regions or the DMN regions in Fox et al. (2005). In the present work, the AAL-based DMN regions were determined primarily according to the coordinates. The ROIs in the AAL-atlas which cover the coordinates or the most adjacent ones were selected. Of them, the peak coordinates (−14, 38, 52)* in the superior frontal (BA8) and (3, −51, 8)* in the retrosplenial (BA30) reported in Fox et al. (2005) are located outside the AAL-atlas of the cerebrum, so we selected their two most adjacent coordinates inside the AAL-atlas, which were (−14, 38, 50) and (3, −45, 11) located in Frontal_Sup_L and Cingulum_Post_R, respectively. Because the two coordinates (−3, 39, −2) and (1, 54, 21) are adjacent to the inter-hemisphere locations between the left and right homogeneous regions, the corresponding bilateral AAL-atlas regions were also selected. The peak coordinate (−2, −36, 37)* is near the boundary between cingulum_Mid_L and cingulum_Post_L, but the great part of the left PCC in Fox et al. (2005) is included in cingulum_Post_L, so we selected cingulum_Post_L as the corresponding left PCC.

scopes in a network (Latora and Marchiori, 2001, 2003). Such metrics are essentially well-defined versions of the classical small-world metrics of the characteristic path length and clustering coefficient, irrespective of the network connectivity. Of them, the global efficiency could be interpreted as inversely related to the characteristic path length while the local efficiency is a generation of the clustering coefficient. Studies have applied them into estimating economical performance of small-world cortical anatomical networks of cat and macaque (Latora and Marchiori, 2001) and functional networks of human brains (Achard and Bullmore, 2007; Wang et al., 2009). In the present work, we therefore favored the use of global and local efficiencies to compare the small-world topology between different behavioral states. The following are their formula definitions in a graph G with N nodes (Achard and Bullmore, 2007; Ginestet et al., 2011; Latora and Marchiori, 2001, 2003),

$$E_{global}(G) = \frac{1}{N(N-1)} \sum_{i \in G} \sum_{j \neq i \in G} d_{ij}^{-1}$$

where d_{ij} denotes the shortest path distance from nodes i to j ;

$$E_{local}(G) = \frac{1}{N} \sum_{i \in G} E_{global}(G_i)$$

where G_i denotes a subgraph of G , containing all the nearest neighbors of node i .

Moreover, the region-specific global efficiency, denoted by $E_{nodal_global}(i)$, is also required,

$$E_{nodal_global}(i) = E_{global}(G, i) = \frac{1}{N-1} \sum_{j \neq i \in G} d_{ij}^{-1}$$

which quantifies the connectivity of node i to all the other nodes in the graph (Ginestet et al., 2011).

To estimate the small-world properties, we generated 100 degree-matched random networks by a Markov-chain algorithm (Maslov and Sneppen, 2002; Milo et al., 2002; Sporns and Zwi, 2004). These metrics (E_{global} and E_{local}) of real networks were normalized by calculating the ratios with the mean values from the corresponding 100 random networks. As originally proposed by Watts and Strogatz (1998), small-world networks have short characteristic path lengths (similar to random networks) and high clustering coefficients (similar to regular networks). Correspondingly, the global efficiency of a small-world network should be approximately equal to that of the degree-matched random networks while the local efficiency is much higher ($E_{global_real}/E_{global_random} \approx 1$, $E_{local_real}/E_{local_random} > 1$), and these features have been demonstrated in small-world brain functional networks (Achard and Bullmore, 2007).

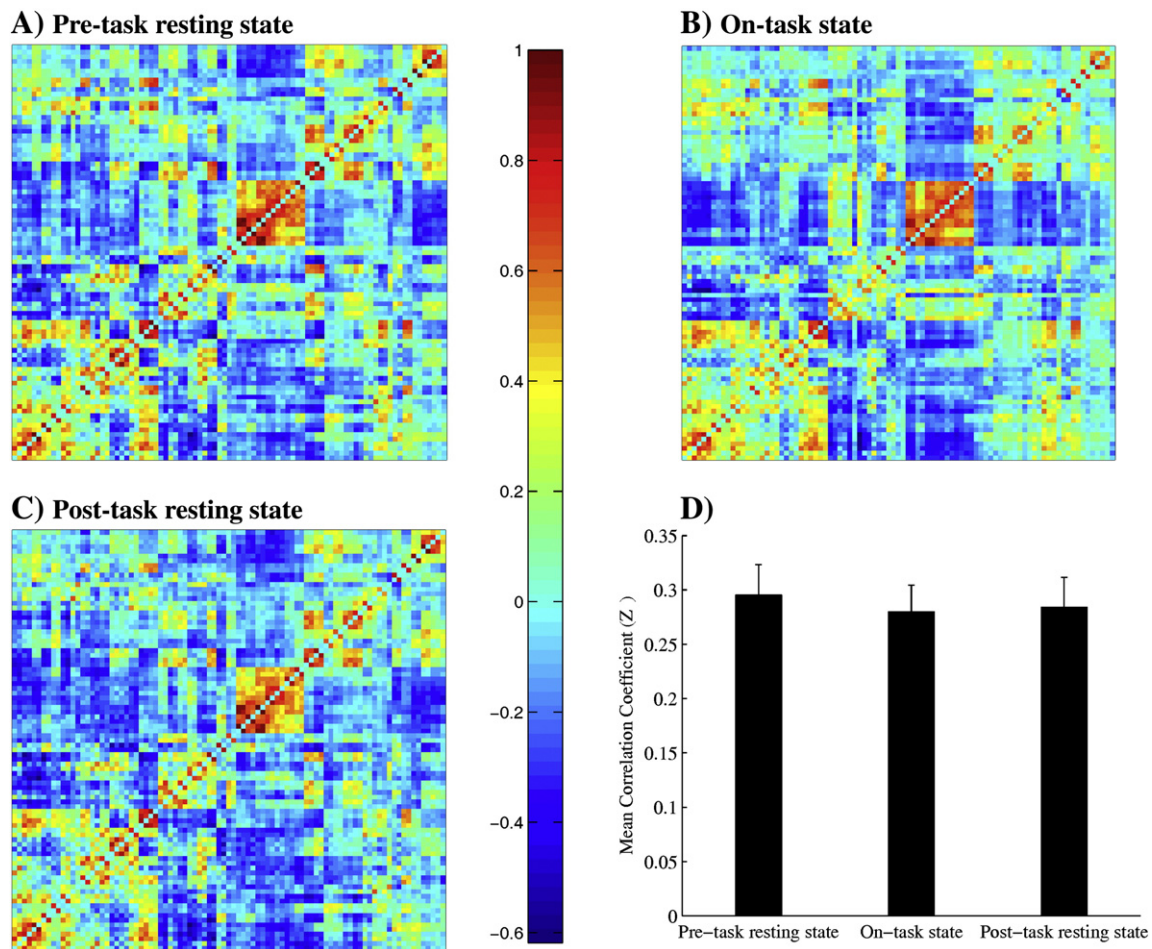


Fig. 2. Mean inter-regional correlation matrices and mean correlation coefficients (Z-values) during the pre-task resting, on-task and post-task resting states, respectively. The mean inter-regional correlation matrices were obtained by averaging a set of correlation matrices across subjects during the pre-task resting (A), on-task (B) and post-task resting states (C), respectively, where individual correlation matrix was acquired by calculating Pearson correlation coefficients of time series between each pair of AAL brain regions. The color bar indicates the correlation coefficients. D: the density or mean correlation coefficients of inter-regional correlation matrices (after Fisher's r -to- z transformation for each subject) were obtained during the three states, by taking the mean over all positive connections and over subjects, respectively. There was no significant difference in density among the three behavioral states (ANOVA, $F=1.34$, $df=2$, $P=0.273$).

Statistical analysis

Threshold selection

In the present study, we employed flexible correlation thresholds $T (\geq 0)$ to generate large-scale functional networks for each of the three behavioral states with exactly the same number of nodes and edges or connectivity, ensuring that any graph differences between states would be really due to reconfiguration of specific functional connectivity, not the overall connectivity in network topology. A measurement of threshold, the sparsity S of brain networks, is usually defined by a ratio of the number of existing edges over maximum possible number of edges. Then, the differences in network topology between states were further statistically evaluated by fixing the sparsity ($0.05 \leq S \leq 0.46$, step by 0.01). The minimum S of 0.05 was empirically set (Achard et al., 2006; Wang et al., 2009; Watts and Strogatz, 1998), while the maximum S of 0.46 was determined by the minimum value of the 45 maximum S values (when $T=0$) across all subjects and states (15 subjects \times 3 states). As a result, a set of large-scale brain functional networks (totally 42) were generated for each subject during each state over a wide range of sparsity ($0.05 \leq S \leq 0.46$).

Statistical comparisons

To determine whether there were significant differences in the small-world properties (E_{global_real} , E_{local_real} , $E_{global_real}/E_{global_random}$, and $E_{local_real}/E_{local_random}$) of brain functional networks, the global DMN topography and its two nodal graph properties (degree and E_{global_real} of the fourteen DMN regions) between two states (the on-task state or the post-task resting state vs. the pre-task resting state), two-tailed paired t-tests were performed for each statistic across subjects. Of note, multiple statistical tests of the between-state differences in the small-world and DMN nodal properties were respectively corrected over a wide range of sparsity levels in achieving an overall significance level ($P < 0.05$) via Monte-Carlo simulation, except the global DMN topography. As a result, two groups of multiple-comparison matrices, i.e., 4 small-world metrics \times 42 sparsity levels and 28 metrics (fourteen DMN regions by two nodal graph properties) \times 42 sparsity levels, were available in between-state comparisons.

Our aim of the statistical evaluation is to find significant ranges of sparsity levels of true differences in topological metrics. Here, we made use of a scheme of Monte-Carlo correction in detection of truly activated brain regions in functional studies (Forman et al., 1995; Ledberg et al., 1998; Xiong et al., 1995; AlphaSim program in AFNI software package: <http://afni.nimh.nih.gov/>). In the present work, the basic hypothesis is that the true differences in topological metrics between states would cover a wide range of sparsity levels (namely, sparsity segments), whereas random noise should have much less of a tendency to form a widely enough significant sparsity segment. Thus, an appropriate combination of thresholding on both individual sparsity significance level (p) of each testing statistic and sparsity segment length (SSL , the number of sparsity levels in a range of sparsity) could be used as criteria to distinguish between truly

significant differences and random noise. First, we presented estimates of false positive probability distributions for sparsity segments as a function of SSL and p via Monte-Carlo simulations (3000 iterations in the

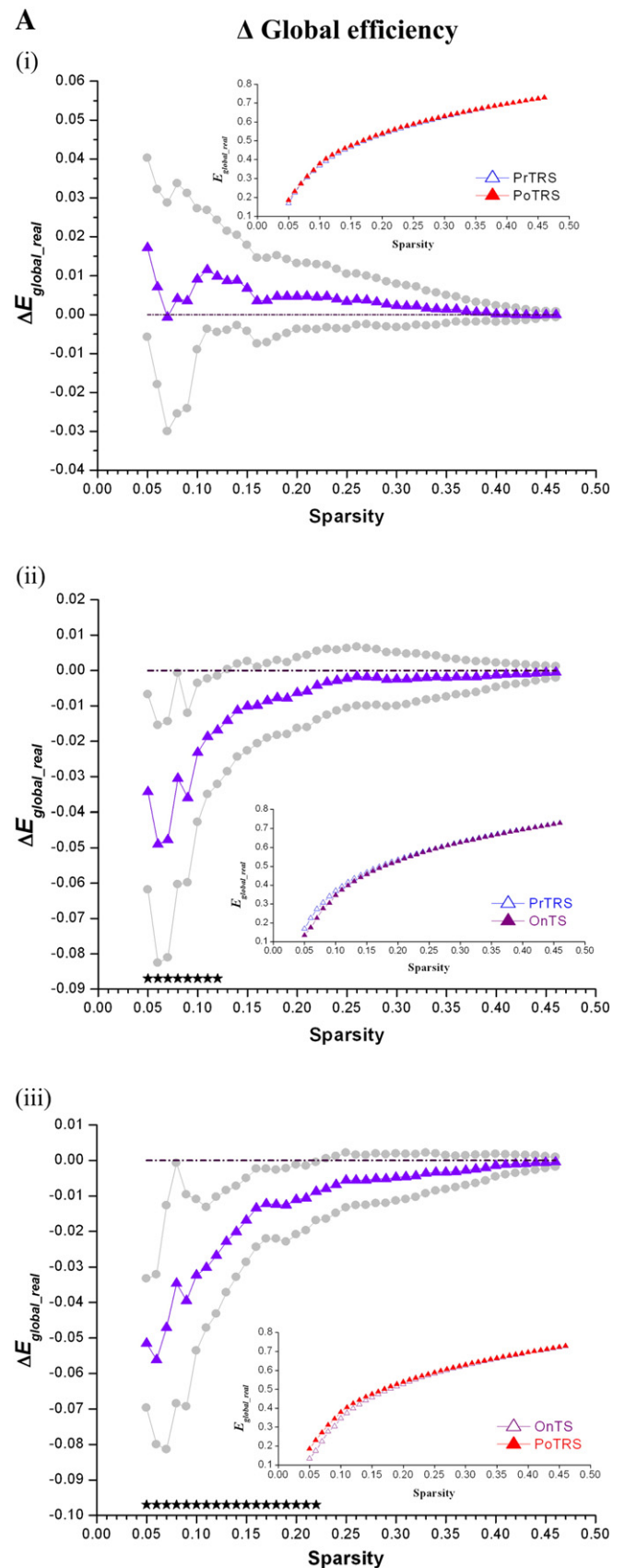


Fig. 3. Between-state comparisons of small-world properties as functions of sparsity. The graphs show the differences in the small-world properties between states (i: the post-task resting state vs. the pre-task resting state; ii: the on-task state vs. the pre-task resting state; iii: the on-task state vs. the post-task resting state) as functions of sparsity. The gray lines represent the 95% confidence intervals of the between-state differences over the range of sparsity. The solid stars indicate there are multiple significant differences in the small-world properties between states ($P < 0.05$, Monte-Carlo corrected, individual sparsity significance level $p = 0.05$, $SSL \geq 3$), while the hollow stars indicate individual significance levels (individual $p < 0.05$, uncorrected). All the insets show original values of the small-world properties during each state (In all insets, red lines: post-task resting state (PoTRS); fuchsia lines: on-task state (OnTS); blue lines: pre-task resting state (PrTRS)). A: the global efficiency (E_{global_real}); B: the local efficiency (E_{local_real}); C: the normalized global efficiency ($E_{global_real}/E_{global_random}$); D: the normalized local efficiency ($E_{local_real}/E_{local_random}$).

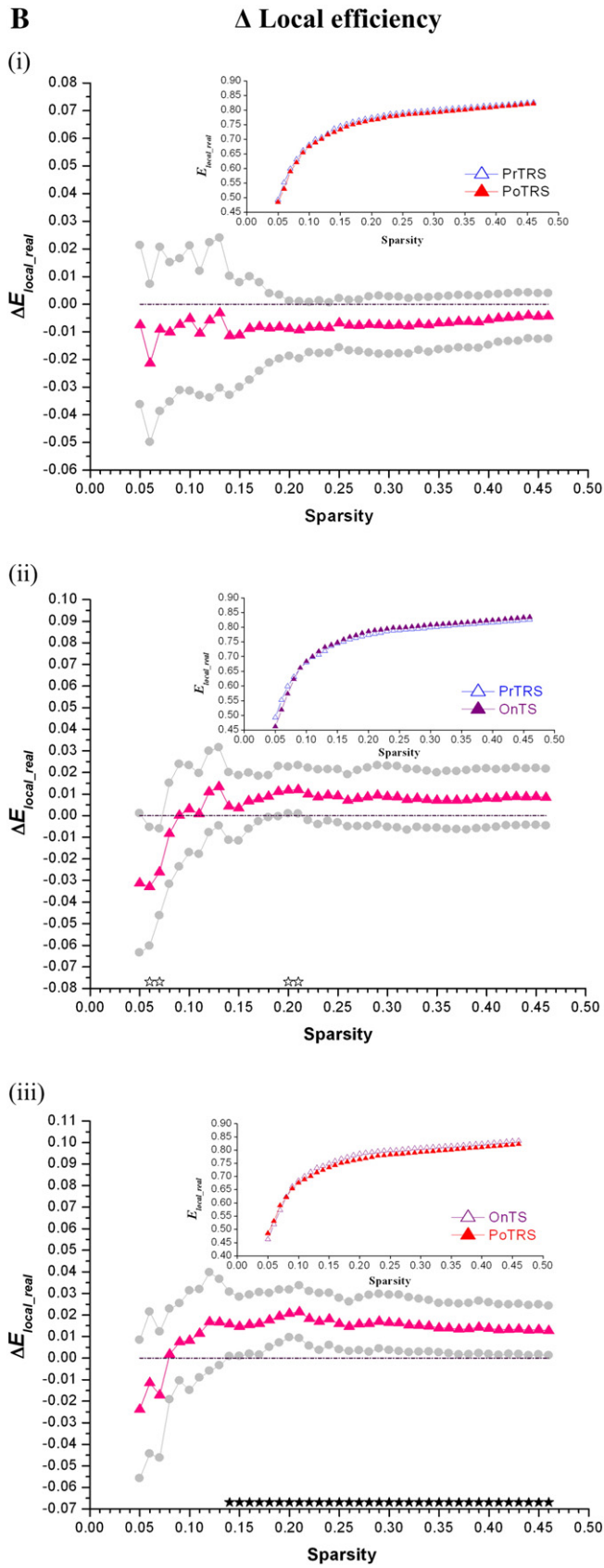


Fig. 3 (continued).

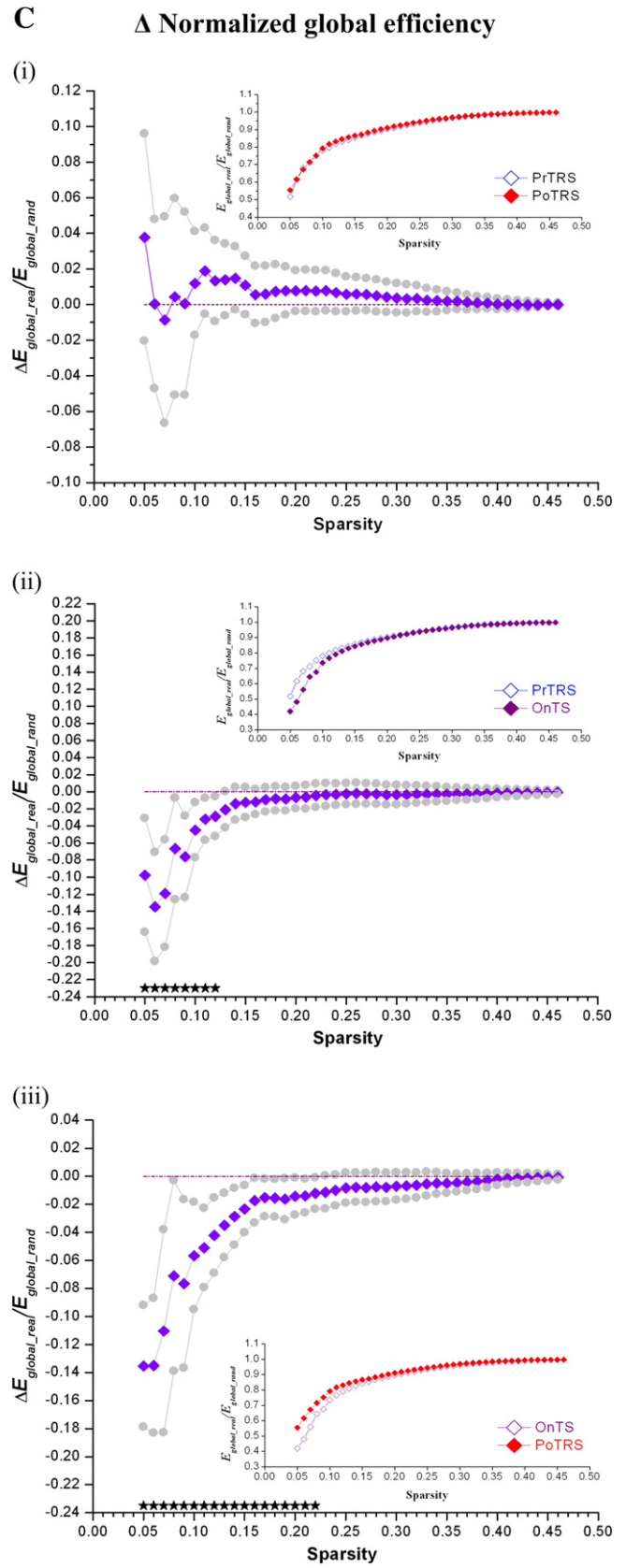


Fig. 3 (continued).

present work) for the two multiple-comparison matrices (4×42 and 28×42), respectively. Then, we decided an appropriate combination of SSL and p thresholds whose corresponding estimate of false positive

probability was less than 0.05. Consequently, we acquired significant sparsity segments of true differences under a desired overall significance level, $P < 0.05$.

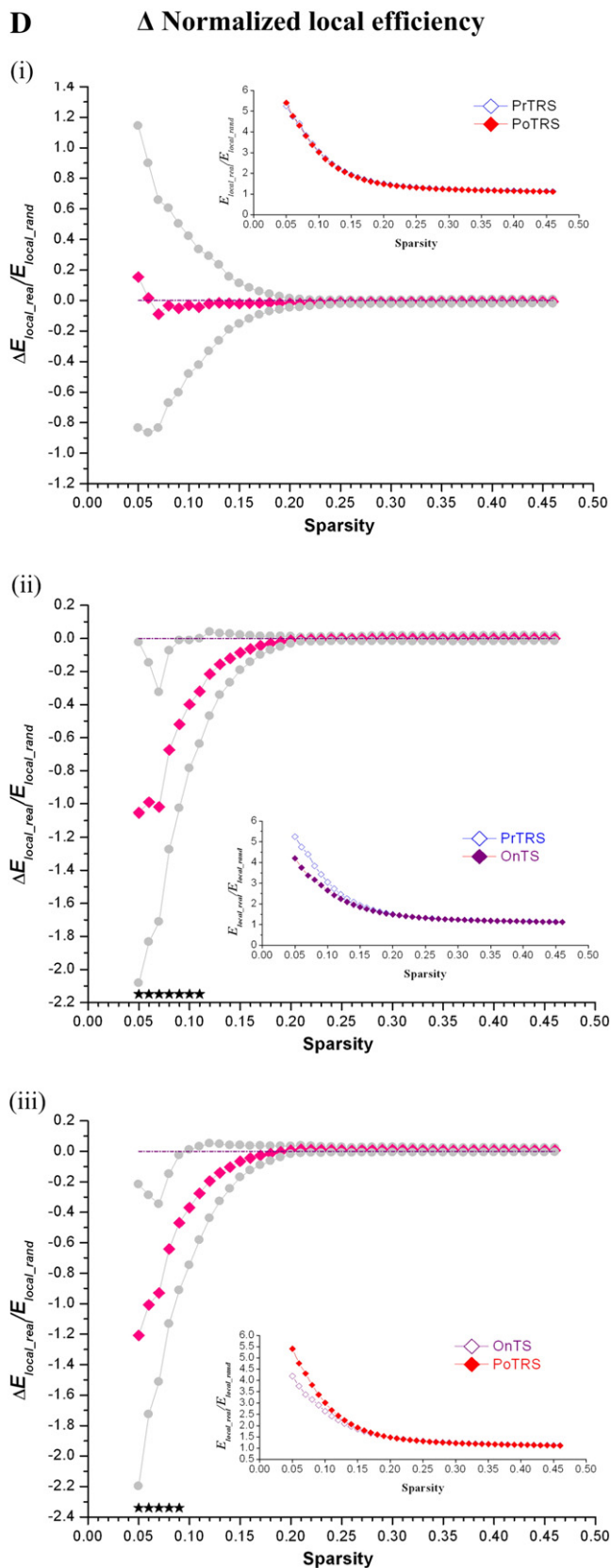


Fig. 3 (continued).

Table 3
Small-world comparisons of the brain functional networks.

Relations	E_{global_real}	E_{global_real}	$E_{global_real}/E_{global_random}$	$E_{global_real}/E_{global_random}$
<OnTS, PrTRS>	<	NA	<	<
<OnTS, PoTRS>	<	>	<	<
<PoTRS, PrTRS>	≈	≈	≈	≈

The table shows summarized results of the small-world comparison analysis in Fig. 3, i.e., during the on-task state (OnTS) vs. the pre-task resting state (PrTRS), during the OnTS vs. the post-task resting state (PoTRS), and during the PoTRS vs. the PrTRS. In addition, “NA” means that the relationship of the OnTS and the PrTRS in terms of E_{local_real} could not be determined in the current data. Because in Fig. 3B-ii, the differences of E_{local_real} between the OnTS and the PrTRS are only individual significant at some sparsity levels ($S = 0.06, 0.07, 0.20$ and $0.21, p < 0.05$, uncorrected), and were regarded as random noise in terms of the present Monte-Carlo correction.

Results

No significant difference in density of inter-regional correlation matrices across states

Differences in density of inter-regional correlation matrices between different conditions can be tested by considering the mean correlation coefficients over all studied connections (Ginestet and Simmons, 2011). Figs. 2A–C shows the mean inter-regional correlation matrices across subjects based on the AAL-atlas during the pre-task resting, on-task and post-task resting states, respectively. Fig. 2D shows the density or mean correlation coefficients of inter-regional correlation matrices (after Fisher’s r-to-z transformation for each subject) during the three states, each of which was acquired by taking the mean over all positive connections and over subjects. There was no significant difference in density among the three behavioral states (ANOVA, $F = 1.34, df = 2, P = 0.273$).

Robustness of the small-world topology across states

Fig. 3 shows that the brain functional organization has a robust, efficient small-world configuration ($E_{global_real}/E_{global_random} \approx 1, E_{local_real}/E_{local_random} > 1$) across the pre-task resting, on-task and post-task resting states within a wide range of sparsity levels ($0.05 \leq S \leq 0.46$), characterized by both high global and local efficiencies (E_{global_real} and E_{local_real}). Consistently, the small-world topology has been demonstrated in previous brain functional network studies during both rest (AAL-based fMRI: Achard and Bullmore, 2007; Achard et al., 2006; Salvador et al., 2005a; Wang et al., 2009; voxel-based fMRI: Van den Heuvel et al., 2008) and task (fMRI: Eguíluz et al., 2005; Ginestet and Simmons, 2011; EEG: Micheloyannis et al., 2006; MEG: Bassett et al., 2006). Taken together, our data demonstrated that the small-world configuration of brain functional organization was robust across task and resting states.

Stability of the small-world topology across the pre-/post-task resting states

There was no significant difference in both global and local efficiencies of the small-world brain functional networks between the pre- and post-task resting states over a wide range of sparsity levels ($0.05 \leq S \leq 0.46$) (see Figs. 3A-i and B-i). When scaled to degree-matched random networks ($E_{global_real}/E_{global_random}$ and $E_{local_real}/E_{local_random}$), the normalized efficiencies had no significant difference between the two resting states either (see Figs. 3C-i and D-i). Our data demonstrated the small-world configuration of brain functional organization was stable during resting states regardless of preceding experiences.

Changes in the small-world topology during the on-task state

There were significant differences in both global and local efficiencies of small-world brain functional networks during the on-task state

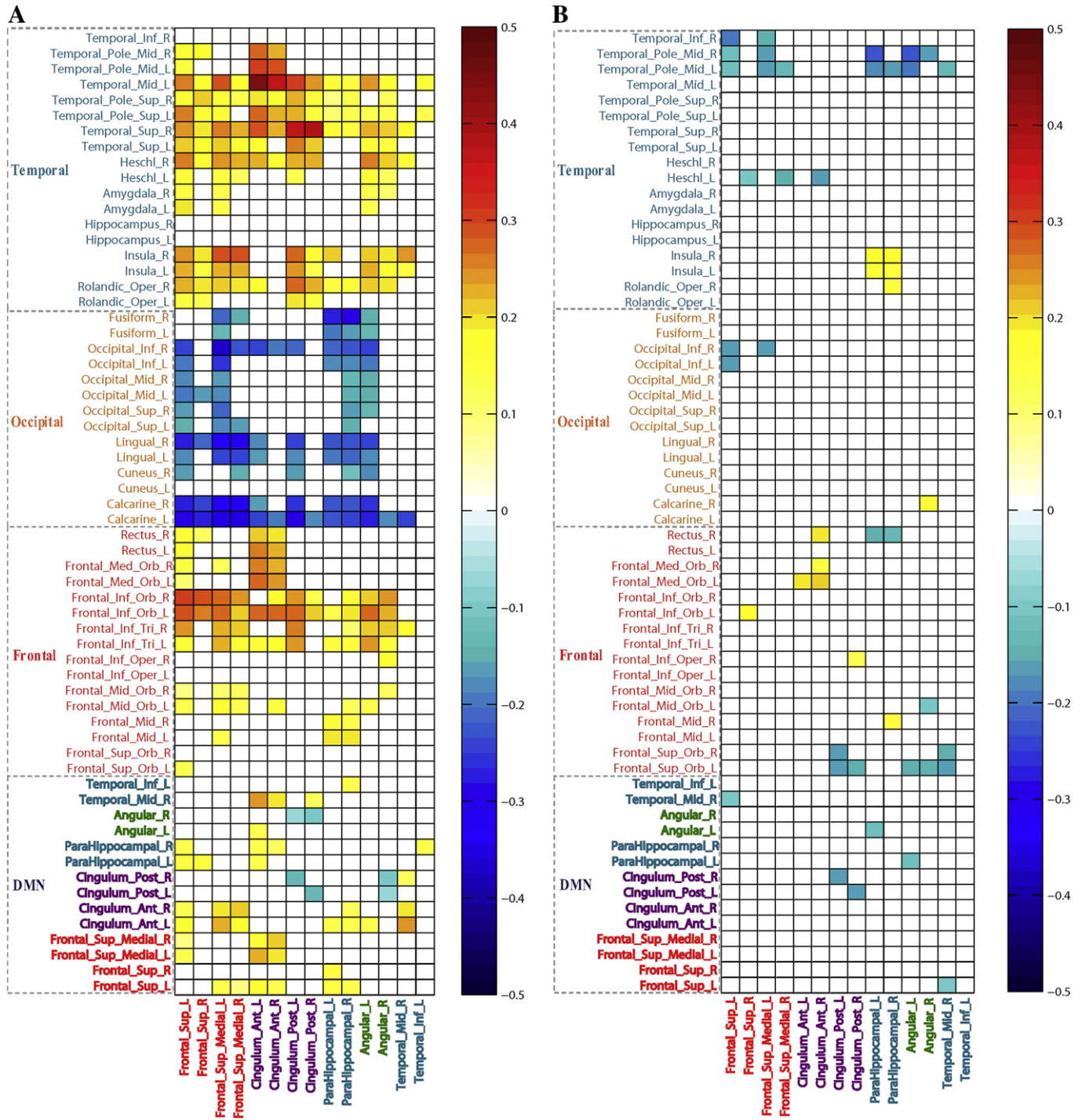


Fig. 4. The variation maps of the global DMN topography. A: changes of the on-task state relative to the pre-task resting state; B: changes of the post-task resting state relative to the pre-task resting state; Color cells indicate the individual significant differences in the global DMN topography between the task-driven states and pre-task resting state (individual $p < 0.05$, uncorrected). Warm color cells represent positive values while cold color cells represent negative values.

compared with the pre- and post-task resting states within some ranges of sparsity (see Figs. 3A-ii, iii and B-ii, iii). When scaled to degree-matched random networks, the normalized efficiencies had significant differences as well (see Figs. 3C-ii, iii and D-ii, iii). The statistical multiple comparisons of the small-world properties were corrected by the Monte-Carlo simulation ($P < 0.05$, individual $p = 0.05$, $SSL \geq 3$). We found that, as marked by solid stars, during the on-task state compared with the pre- and post-task resting states, E_{local_real} was significantly increased ($0.14 \leq S \leq 0.46$, see Fig. 3B-iii) while E_{global_real} ($0.05 \leq S \leq 0.12$, see

Fig. 3A-ii; $0.05 \leq S \leq 0.22$, see Fig. 3A-iii), $E_{global_real}/E_{global_random}$ ($0.05 \leq S \leq 0.12$, see Fig. 3C-ii; $0.05 \leq S \leq 0.22$, see Fig. 3C-iii) and $E_{local_real}/E_{local_random}$ ($0.05 \leq S \leq 0.11$, see Fig. 3D-ii; $0.05 \leq S \leq 0.09$, see Fig. 3D-iii) were significantly diminished. For E_{local_real} in Fig. 3B-ii, the hollow stars indicate individual significant differences between the on-task state and pre-task resting state at some sparsity levels ($S = 0.06, 0.07, 0.20$ and 0.21 , $p < 0.05$, uncorrected), and these differences were regarded as random noise in terms of the present Monte-Carlo correction. All the comparison results in Fig. 3 were summarized in Table 3.

Changes in the global DMN topography during the task-driven states

Compared with the pre-task resting state, the variations of the global DMN topography during both on-task state and post-task resting state are shown in Figs. 4A and B (individual $p < 0.05$, uncorrected), respectively. The 90 AAL regions are classified into six partitions: the frontal, parietal, occipital, temporal, cingulum and subcortical areas. Of note, the DMN components are listed independently as a separated module. A semantic-matching task primarily demands the involvement of visual and semantic processing, so we just showed the variation maps of functional connectivity between the DMN and frontal, occipital and temporal areas in this article.

During the on-task state vs. the pre-task resting state (see Fig. 4A), most of the varied intra-DMN functional connectivity (except among cingulum_Post_L, cingulum_Post_R and angular_R) was predominantly intensified. The varied extra-DMN functional connectivity associated with the frontal-temporal areas was predominantly intensified, while others associated with the occipital lobes was predominantly decreased. However, during the post-task resting state vs. the pre-task resting state (see Fig. 4B), the intra-DMN functional connectivity between cingulum_Post_L and cingulum_Post_R was decreased, which also occurred during the on-task state. In the extra-DMN connectivity topography, several regions in the frontal-temporal area such as the superior orbito-frontal and middle temporal pole regions exhibited reduced functional connectivity with the DMN system as well.

Changes in the DMN nodal graph properties during the task-driven states

Most of the DMN nodal degrees were significantly increased during the on-task state relative to the pre-task resting state within some ranges of sparsity levels (see Fig. 5A, $P < 0.05$, Monte-Carlo corrected, individual $p = 0.05$ and $SSL \geq 4$). Only four DMN regions exhibited no significant difference in nodal degree, including Temporal_Inf_L, Angular_R, Cingulum_Post_R and Parahippocampal_L. However, during the post-task resting state vs. the pre-task resting state (see Fig. 5B, $P < 0.05$, Monte-Carlo corrected, individual $p = 0.05$ and $SSL \geq 4$), the degree of Parahippocampal_L was significantly decreased while the degrees of Parahippocampal_R and Cingulum_Ant_R were significantly increased within some ranges of sparsity levels. Thus, the degree of Parahippocampal_L was maintained across the pre-task resting state and on-task state, but was significantly decreased during the post-task resting state. The degrees of Parahippocampal_R and Cingulum_Ant_R were significantly increased in both the task-driven states relative to the pre-task resting state. In addition, most of the DMN regions with nodal degree increased were also increased in global efficiency (see Fig. 5).

Discussion

In the present study, we investigated the robustness and plasticity of the brain intrinsic functional architecture of coherent spontaneous

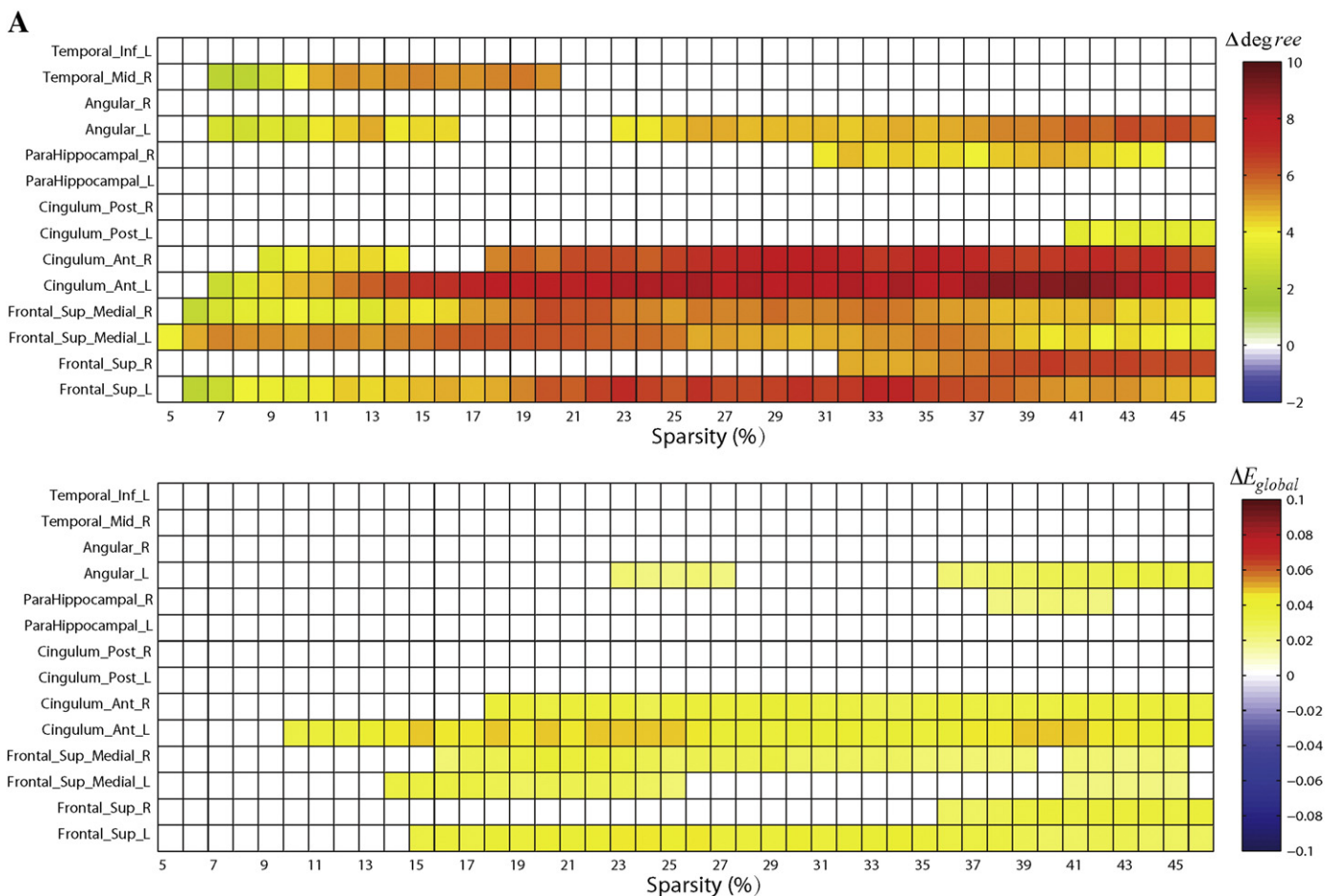


Fig. 5. The variation maps of the DMN nodal graph properties (degree and global efficiency) as functions of sparsity. A: changes of the on-task state relative to the pre-task resting state; B: changes of the post-task resting state relative to the pre-task resting state. All the differences of the DMN nodal graph properties were statistically tested by two-tailed paired t-tests between states over a wide range of sparsity levels, and the multiple significances of (A) and (B) were corrected by the Monte-Carlo simulation, respectively ($P < 0.05$, Monte-Carlo corrected, individual sparsity significance level $p = 0.05$, $SSL \geq 4$). Warm color cells represent positive values while cold color cells represent negative values.

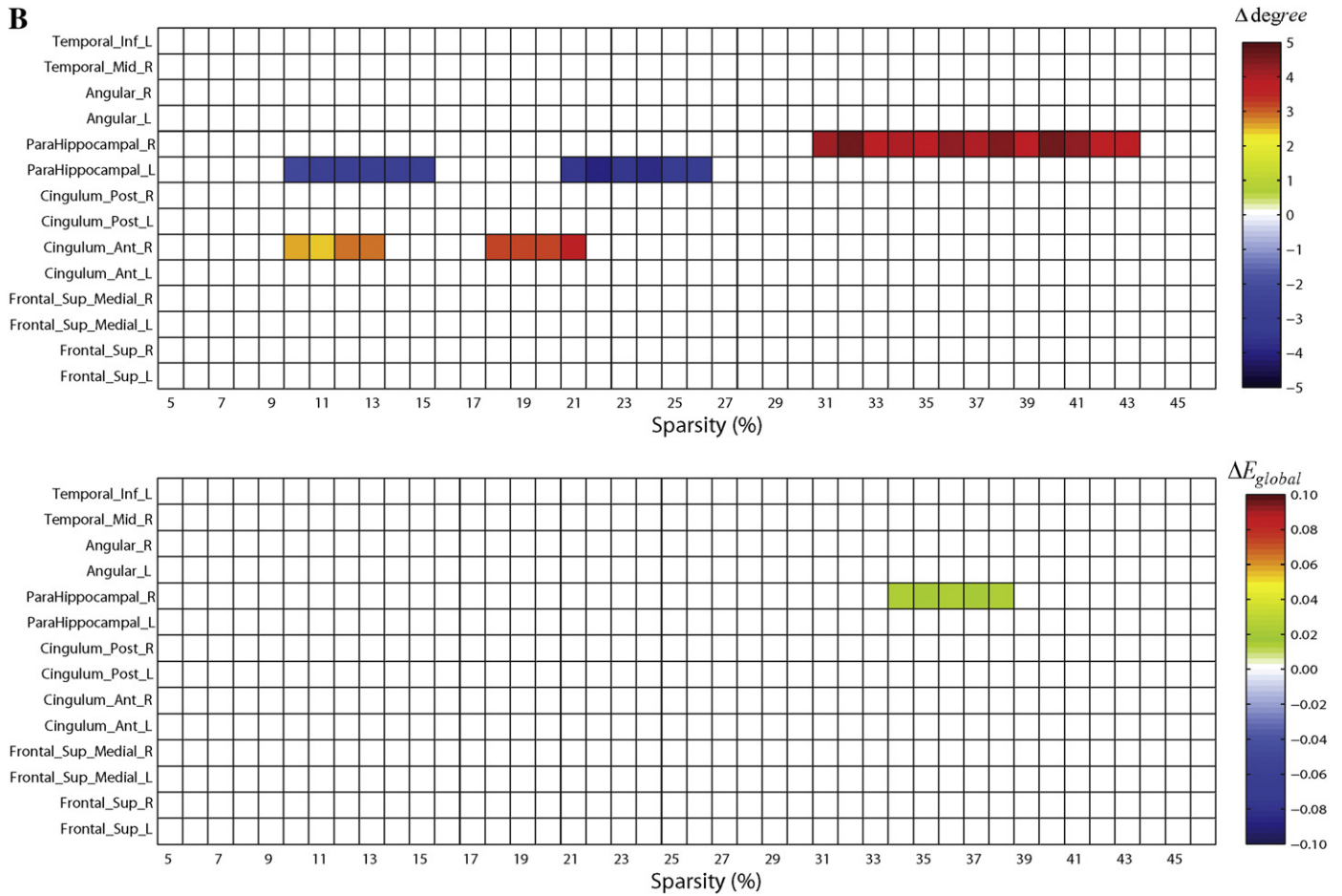


Fig. 5 (continued).

activity across task and resting states in several topologies. To our best knowledge, we for the first time investigated the topological changes in the large-scale intrinsic functional organization in both task-driven states through three levels: (a) the whole brain small-world topology, (b) the global DMN topography, and (c) the DMN nodal graph properties. Before doing these, we also reported there was no significant difference in the mean correlation coefficients or density of inter-regional correlation matrices among the three states (see Fig. 2D). Moreover, we fixed a wide range of sparsity of brain networks for the statistical evaluation of differences in the small-world and DMN nodal properties between states. It appeared that these processes allowed to disentangle differences of intrinsic connectivity in topology from differences in inter-regional correlation density. Finally, we revealed some development features in topology of the brain functional intrinsic organization in both task-driven states, and may provide further insights into dynamic task-driven processes of coherent spontaneous activity over states.

Robustness and stability of the small-world topology across the pre-/post-task resting states

Our results indicated that, during the pre-/post-task resting states, the brain functional organization maintained a robust, stable and efficient small-world configuration for its internal complicated information processing (see Figs. 3A–D–i). A small-world topology has been demonstrated in previous brain functional network studies during a continuous resting state (AAL-based fMRI: Achard and Bullmore, 2007; Achard et al., 2006; Salvador et al., 2005a; Wang et al., 2009; voxel-based fMRI: Van den Heuvel, et al., 2008). In the present

work, we further found that the post-task processes could not induce disturbances on the intrinsic small-world topology or the balance between the local specialization and global integration. Thus, the efficient small-world configuration of the brain organization may remain robust and stable across different resting states (or passive states) regardless of recent experiences. However, we cannot conclude that the two resting states are equivalent, because their differences could be uncovered by the DMN topological analysis in the later sections.

Changes in the small-world topology during the on-task state

The results indicated that the task-induced functional organization of the human brain also had an efficient small-world configuration (see Figs. 3A–D–ii, iii), which is robust in general. The small-world organization has been demonstrated in previous brain functional network studies during a task (fMRI: Eguíluz et al., 2005; Ginestet and Simmons, 2011; EEG: Micheloyannis et al., 2006; MEG: Bassett et al., 2006). However, we found significant differences in the small-world properties (E_{local_real} , E_{global_real} , $E_{global_real}/E_{global_random}$, and $E_{local_real}/E_{local_random}$) between the on-task state and resting states (see Figs. 3A–D–ii, iii or Table 3). These findings indicated that the ongoing task could impact the intrinsic small-world configuration of the human brain. Moreover, the small-world organization reflects an optimal balance between the local specialization and global integration of parallel information processing (Bassett and Bullmore, 2006; Sporns and Zwi, 2004; Sporns et al., 2004). Therefore, there would be a new optimal balance between the functional segregation and integration adaptively generated in support of the task performance.

Rubinov and Sporns (2010) suggests that local efficiency is a measure of functional segregation for the ability of specialized processing to occur within densely interconnected groups of brain regions. Global efficiency is a measure of functional integration for the ability of rapidly combining specialized information over distributed brain regions. On the one hand, the current data demonstrated that the average local efficiency (E_{local_real}) was increased during the on-task state (see Figs. 3B–ii, iii), that is, there was higher efficient recurrent processing in the local circuitries. The normalized local efficiency ($E_{local_real}/E_{local_random}$) was diminished (see Figs. 3D–ii, iii), which may indicate that the efficiency of local synchronous couplings was closer to that of the corresponding random networks in favor of more efficient task-related subprocesses. Therefore, the brain may exhibit stronger advantages in the local specialized information processing during the task performance. On the other hand, both the original and normalized global efficiency (E_{global_real} and $E_{global_real}/E_{global_random}$) were decreased during the on-task state (see Figs. 3A–ii, iii and C–ii, iii). These findings implied that the average sequence of functional associated regions over the whole cortex was longer under the active task stimulus. Moreover, more multiple series of local specialized information processing were involved in the task-related processes. However, as an opposite of the information efficiency, the information diversity of the global integration tended to be increased at the same time in favor of a diverse task-related global integration from more widely distributed sources of local specialized information. Hence, the distinct changes in the local and global efficiencies may reflect adaptive modulation of the balance between the functional segregation and integration in the brain. On the whole, the large-scale small-world configuration of brain functional organization was robust over states, while with adaptive dynamic properties of local and global efficiencies.

Finally, a pioneer work by Bassett et al. using MEG found that the whole brain small-world properties were not much affected by a visually cued finger tapping task (Bassett et al., 2006). In addition to the limitations (see the Introduction section of the paper), the simply-repeated motion task may induce some reshaped local spatial patterns rather than global topological properties in the large-scale intrinsic organization. Thus, we speculate that the intrinsic small-world configuration could not be modulated by such simply-repeated motion or sensory tasks. But the active semantic-matching task impacted the intrinsic small-world configuration during the on-task state, which may demand more cognitive processing and brain areas engagement. So, the small-world topological properties of brain functional networks may be strongly related to task properties.

Changes in the global DMN topography during the task-driven states

In addition to the small-world analysis with a macroscopic perspective in view of graph theories, the global DMN topography was also needed for analysis as a pivotal subsystem within the large-scale intrinsic organization. Previous studies have demonstrated that the spatial patterns within the DMN are sensitive to different behavioral states (Fransson, 2006; Hasson et al., 2009; Tambini et al., 2010; Waites et al., 2005). In the present study, it was demonstrated that the global DMN topography was changed in both task-driven states, because the DMN may be essentially engaged during both task and post-task processes.

Studies have demonstrated strong relationship between the DMN and cognition performance. For instance, abnormality of the DMN in schizophrenia patients could result in a relatively poor performance of working memory task (Whitfield-Gabrieli et al., 2009). Reduction in the DMN activity occurs with cognition decline during normal aging (Damoiseaux et al., 2008). Performance on a working memory task is positively correlated with the strength of functional connectivity between the medial frontal gyrus or ventral anterior cingulate cortex (MFG/vACC) and PCC (Hampson et al., 2006). Moreover, Hampson et al. (2006) suggest that the DMN may be engaged during cognitive tasks to facilitate or monitor cognitive performance. Our results further suggest a consistent perspective from the changes in both extra- and

intra-DMN functional connectivity during the on-task state. First, the reduction in functional connectivity between the occipital and DMN areas (see Fig. 4A) may indicate that the task-relevant visual occipital areas performed weaker synchronization with the DMN system during the on-task state. Hasson et al. (2009) also found weaker synchronization between the DMN and task-relevant regions during task performance. The reduction in the extra-DMN functional connectivity may reflect a competition of the processing resources allocation between the DMN and some task-relevant regions in the brain. Second, the functional connectivity between the DMN and frontal-temporal areas predominantly skewed towards relatively greater levels during the on-task state (see Fig. 4A). This finding could be interpreted as reflecting a facilitating synchronous interference between the DMN and frontal-temporal areas for the purpose of the task-relevant semantic processing and the control of memory information retrieval. Third, most of the varied intra-DMN functional connectivity (except among cingulum_Post_L, cingulum_Post_R and angular_R) was also found to be significantly enhanced during the on-task state (see Fig. 4A). This finding reflects stronger coupling coordination within the DMN, which may be related to task-relevant information encoding or a reflection of internal mediating processes. Hence, the DMN may be essentially engaged during task performance in specific fashions rather than absolutely suppressed.

We also found a weaker synchronization in the PCC-angular network within the DMN during the on-task state, and the decreased connectivity between the bilateral PCC persisted across both the task-driven states (see Fig. 4). It accords well with previous studies demonstrating substantially weaker functional connectivity based on a seed region of PCC/precuneus within the DMN during a task than rest (Fransson, 2006; Hasson et al., 2009). The PCC or PCC-angular network may be related to active disengagement from ongoing or previous tasks (Hasson et al., 2009). On the whole, both active engagement and disengagement of the DMN regions are behaviors of task-driven adaptations over states.

During the post-task resting state, there was slightly specific reconfiguration in the global DMN topography. Two opposite modes of variations occurred in the global DMN topography, and they may conflict with each other. One was a recurrence of the varying functional connectivity associated with the preceding task. For example, during both the task-driven states vs. the pre-task resting state, the functional connectivity between the bilateral PCC was decreased, or the functional connectivity between Cingulum_Ant_L/R and Frontal_Med_Orb_L was enhanced (see Fig. 4). The other one was a reverse changing of functional connectivity relative to the on-task state. For example, the functional connectivity between the DMN and frontal-temporal areas was predominantly intensified during the on-task state (see Fig. 4A), but some regions in the frontal-temporal area exhibited reduced functional connectivity with the DMN during the post-task resting state (see Fig. 4B).

Recently, there is a serious debate about the nature of default mode activity. Several researchers suggest that this intrinsic activity in the DMN is associated with task-unrelated thoughts (Masson et al., 2007; McKiernan et al., 2006), or likely reflect a more fundamental property of the brain functional organization (Raichle and Snyder, 2007; Vincent et al., 2007). By contrast, some studies have proposed that this activity at rest could be associated with recent experiences (Hasson et al., 2009; Miall and Robertson, 2006; Tambini et al., 2010). In the present study, the common variations in the global DMN topography between the on-task state and post-task resting state seem to be evidence on their close association. The opposite variations in the global DMN topography during the post-task resting state relative to the on-task state might be related to a recovery of task-free default mode activity. Previous studies have also demonstrated reshaped resting-state functional connectivity patterns after cognitive tasks in human brains (Albert et al., 2009; Hasson et al., 2009; Lewis et al., 2009; Tambini et al., 2010). Albert et al. (2009) and Lewis et al. (2009) related the post-task modulation in the resting-state functional connectivity to the recent learning experiences. In the present study, we did not quantitatively measure how

much learning effect occurred during the task performance. Nonetheless, the preceding task could induce changes in the global DMN topography, and the DMN should be strongly engaged in the post-task processes.

Changes in the DMN nodal graph properties during the task-driven states

In addition to the small-world and global DMN topography analysis, changes in the DMN nodal properties were further investigated in terms of nodal degree and global efficiency. A nodal degree can reflect a local association capability of the given node while the nodal global efficiency can reflect a transfer capability over the whole network. On the basis of graph theories, these DMN nodal properties could provide nodal-level evidence on the changes of the DMN activities in both task-driven states, and further supported our hypothesis that the DMN may be essentially engaged during both task and post-task processes.

Our results showed that the nodal degree and global efficiency were significantly increased for most of the DMN regions during the on-task state (see Fig. 5A). These results indicated that the capabilities of both local association and global transfer of the DMN were predominantly increased. Thus, there was denser information integration or distributed cognitive coordination mediated through the DMN. Moreover, hubs play pivotal roles in the coordination of information flow in brain networks (Sporns et al., 2007). Studies have demonstrated a portion of cortical hubs or cores as the components of the DMN in both brain structural (Hagmann et al., 2008) and functional networks over passive and active on-task states (Buckner et al., 2009). In addition, the DMN may also play a critical role in different cognitive abilities (Damoiseaux et al., 2008; Hampson et al., 2006; Whitfield-Gabrieli et al., 2009). Therefore, we suggest that the DMN may play a critical role in the task-related information integration over the distributed cortical regions during the on-task state.

Moreover, our results also showed that the bilateral parahippocampus varied discriminately in the sense of nodal degree and efficiency during the post-task resting state. Compared with the pre-task resting state, the degree and efficiency of right parahippocampus were significantly increased in both the task-driven states over a range of sparsity (see Fig. 5). By contrast, the degree of left parahippocampus was significantly decreased only during the post-task resting state (see Fig. 5B). Recent studies have demonstrated that parahippocampus is involved in long-term memory encoding (Schon et al., 2004; Wagner et al., 1998), short-term maintenance of working memory (Luck et al., 2010) and their interaction (Axmacher et al., 2008). Thus, we could interpret the results that the right parahippocampus maintained being engaged in task-related memory encoding across both task-driven states. On the other hand, the left parahippocampus might mainly contribute to a recovery of task-free default mode activity during the post-task resting state, and also it might be indirectly involved in the memory consolidation by interaction with the right parahippocampus.

Further considerations

Several issues remain to be addressed in the future. First, the BOLD signals of all the sessions were filtered into the frequency range of 0.01–0.08 Hz in the present study. But a time-scale or frequency-specific brain functional networks should be considered across sequential behavioral states in the future. Second, other types of cognitive tasks should be employed to examine their topological influences on the large-scale intrinsic functional organization in both task-driven states. Third, it is important to understand the dynamic mechanisms of the DMN within the global functional network. According to the default mode theory, the brain may be constantly monitoring the internal or external environment to support overt behaviors (Miall and Robertson, 2006). Thus, does such drastic variations in the DMN topological properties relate to an occurrence of global topological modulation? Finally, the sparsity step would influence the results of Monte-Carlo simulation. Thus, it should be considered as a variable to improve the flexibility of the

Monte-Carlo multiple correction. Moreover, a recent work has developed cost-integrated topological metrics into network topological comparisons, which seems to have escaped the bias problem of thresholds (Ginestet et al., 2011).

Conclusions

In the present study, we conducted an fMRI experiment with the three sequential periods of pre-task resting, on-task and post-task resting states, and explored the task-driven effect on the dynamic large-scale intrinsic functional organization in both on-task state and post-task resting state. Three hierarchical levels were investigated, including (a) the whole brain small-world topology, (b) the global DMN topography, and (c) the DMN nodal graph properties. The results show that, first, the large-scale small-world configuration of brain functional organization is robust in general, regardless of the behavioral state changing, while it varies with significantly higher local efficiency and lower global efficiency during the on-task state. It may reflect an adaptive, dynamic optimal balance between the functional segregation and integration in the brain over states. Second, the DMN may be essentially engaged during both task and post-task processes with adaptively varied spatial patterns and nodal graph properties, which may be related to memory processing or cognitive resource allocation. Furthermore, the dynamic intrinsic connectivity associated with recent or ongoing demands may play important roles in the evolution of brain organization at a large temporal scale. The present study provides further insights into the robustness and plasticity of the brain intrinsic organization over states, which may be the basis of memory and learning in the brain.

Acknowledgments

The authors are grateful to the anonymous referees for their significant and constructive comments and suggestions, which greatly improved the paper. The authors are also grateful to Dr. Yong He and Dr. Michelle Hampson who kindly discussed some issues on fMRI techniques with us and Dr. Cherry Romano who polished the paper carefully. The work is partially supported by the National Natural Science Foundation of China under grant no. 60875075, Beijing Natural Science Foundation (no. 4102007) and Beijing University of Technology Doctoral Foundation Project (no. 52007999200701).

References

- Achard, S., Bullmore, E.D., 2007. Efficiency and cost of economical brain functional networks. *PLoS Comput. Biol.* 3, e17.
- Achard, S., Salvador, R., Whitcher, B., Suckling, J., Bullmore, E.D., 2006. A resilient, low-frequency, small-world human brain functional network with highly connected association cortical hubs. *J. Neurosci.* 26, 63–72.
- Albert, N.B., Robertson, E.M., Miall, R.C., 2009. The resting human brain and motor learning. *Curr. Biol.* 19, 1023–1027.
- Axmacher, N., Schmitz, D.P., Weinreich, I., Elger, C.E., Fell, J., 2008. Interaction of working memory and long-term memory in the medial temporal lobe. *Cereb. Cortex* 18, 2868–2878.
- Bassett, D.S., Bullmore, E.D., 2006. Small-world brain networks. *Neuroscientist* 12, 512–523.
- Bassett, D.S., Meyer-Lindenberg, A., Achard, S., Duke, T., Bullmore, E.D., 2006. Adaptive reconfiguration of fractal small-world human brain functional networks. *Proc. Natl. Acad. Sci. U. S. A.* 103, 19518–19523.
- Bassett, D.S., Wymbs, N.F., Porter, M.A., Mucha, P.J., Carlson, J.M., Grafton, S.T., 2011. Dynamic reconfiguration of human brain networks during learning. *Proc. Natl. Acad. Sci. U. S. A.* 108, 7641–7646.
- Bianciardi, M., Fukunaga, M., van Gelderen, P., Horovitz, S.G., de Zwart, J.A., Duyn, J.H., 2009. Modulation of spontaneous fMRI activity in human visual cortex by behavioural state. *Neuroimage* 45, 160–168.
- Biswal, B., Yetkin, F.Z., Haughton, V.M., Hyde, J.S., 1995. Functional connectivity in the motor cortex of resting human brain using echo-planar MRI. *Magn. Reson. Med.* 34, 537–541.
- Buckner, R.L., Sepulcre, J., Talukdar, T., Krienen, F.M., Liu, H., Hedden, T., Andrews-Hanna, J.R., Sperling, R.A., Johnson, K.A., 2009. Cortical hubs revealed by intrinsic functional connectivity: mapping, assessment of stability, and relation to Alzheimer's disease. *J. Neurosci.* 6, 1860–1873.
- Bullmore, E.D., Sporns, O., 2009. Complex brain networks: graph theoretical analysis of structural and functional systems. *Nat. Rev. Neurosci.* 10, 186–198.

- Calhoun, V.D., Kiehl, K.A., Pearlson, G.D., 2008. Modulation of temporally coherent brain networks estimated using ICA at rest and during cognitive tasks. *Hum. Brain Mapp.* 29, 828–838.
- Cordes, D., Houghton, V.M., Arfanakis, K., Carew, J.D., Turski, P.A., Moritz, C.H., Quigley, M.A., Meyerand, M.E., 2001. Frequencies contributing to functional connectivity in the cerebral cortex in “resting-state” data. *AJNR* 22, 1326–1333.
- Damoiseau, J.S., Beckmann, C.F., Sanz Arigita, E.J., Barkhof, F., Scheltens, Ph., Stam, C.J., Smith, S.M., Rombouts, S.A.R.B., 2008. Reduced resting-state brain activity in the “default network” in normal aging. *Cereb. Cortex* 18, 1856–1864.
- Eguiluz, V.M., Chialvo, D.R., Cecchi, G.A., Baliki, M., Apkarian, A.V., 2005. Scale-free brain functional networks. *Phys. Rev. Lett.* 94, 018102.
- Fair, D.A., Cohen, A.L., Dosenbach, N.U.F., Church, J.A., Miezin, F.M., Barch, D.M., Raichle, M.E., Petersen, S.E., Schlaggar, B.L., 2008. The maturing architecture of the brain's default network. *Proc. Natl. Acad. Sci. U. S. A.* 105, 4028–4032.
- Fair, D.A., Cohen, A.L., Power, J.D., Dosenbach, N.U.F., Church, J.A., Miezin, F.M., Schlaggar, B.L., Petersen, S.E., 2009. Functional brain networks develop from a “local to distributed” organization. *PLoS Comput. Biol.* 5, e1000381.
- Forman, S.D., Cohen, J.D., Fitzgerald, M., Eddy, W.F., Mintun, M.A., Noll, D.C., 1995. Improved assessment of significant activation in functional magnetic resonance imaging (fMRI): use of a cluster-size threshold. *Magn. Reson. Med.* 33, 636–647.
- Fox, M.D., Raichle, M.E., 2007. Spontaneous fluctuations in brain activity observed with functional magnetic resonance imaging. *Nat. Rev. Neurosci.* 8, 700–711.
- Fox, M.D., Snyder, A.Z., Vincent, J.L., Corbetta, M., Van Essen, D.C., Raichle, M.E., 2005. The human brain is intrinsically organized into dynamic, anticorrelated functional networks. *Proc. Natl. Acad. Sci. U. S. A.* 102, 9673–9678.
- Fox, M.D., Corbetta, M., Snyder, A.Z., Vincent, J.L., Raichle, M.E., 2006. Spontaneous neuronal activity distinguishes human dorsal and ventral attention systems. *Proc. Natl. Acad. Sci. U. S. A.* 103, 10046–10051.
- Fransson, P., 2006. How default is the default mode of brain function? Further evidence from intrinsic BOLD signal fluctuations. *Neuropsychologia* 44, 2836–2845.
- Friston, K.J., 2002. Beyond phrenology: what can neuroimaging tell us about distributed circuitry? *Annu. Rev. Neurosci.* 25, 221–250.
- Friston, K.J., Büchel, C., 2000. Attentional modulation of effective connectivity from V2 to V5/MT in humans. *Proc. Natl. Acad. Sci. U. S. A.* 97, 7591–7596.
- Friston, K.J., Frith, C.D., Liddle, P.F., Frackowiak, R.S., 1993. Functional connectivity: the principal component analysis of large (PET) data sets. *J. Cereb. Blood Flow Metab.* 13, 5–14.
- Ginestet, C.E., Simmons, A., 2011. Statistical parametric network analysis of functional connectivity dynamics during a working memory task. *Neuroimage* 55, 688–704.
- Ginestet, C.E., Nichols, T.E., Bullmore, E.T., Simmons, A., 2011. Brain network analysis: separating cost from topology using cost-integration. *PLoS One* 6, e21570.
- Greicius, M.D., Krasnow, B., Reiss, A.L., Menon, V., 2003. Functional connectivity in the resting brain: a network analysis of the default mode hypothesis. *Proc. Natl. Acad. Sci. U. S. A.* 100, 253–258.
- Hagmann, P., Kaurant, M., Gigandet, X., Thiran, P., Wedeen, V.J., Meuli, R., Thiran, J.P., 2007. Mapping the structural core of human cerebral cortex. *PLoS One* 2, e597.
- Hagmann, P., Cammoun, L., Gigandet, X., Meuli, R., Honey, C.J., Wedeen, V.J., 2008. Mapping the structural core of human cerebral cortex. *PLoS Biol.* 6, e159.
- Hampson, M., Peterson, B.S., Skudlarski, P., Gatenby, J.C., Gore, J.C., 2002. Detection of functional connectivity using temporal correlations in MR images. *Hum. Brain Mapp.* 15, 247–262.
- Hampson, M., Driesen, N.R., Skudlarski, P., Gore, J.C., Constable, R.T., 2006. Brain connectivity related to working memory performance. *J. Neurosci.* 26, 13338–13343.
- Hasson, U., Nusbaum, H.C., Small, S.L., 2009. Task-dependent organization of brain regions active during rest. *Proc. Natl. Acad. Sci. U. S. A.* 106, 10841–10846.
- He, Y., Chen, Z.J., Evans, A.C., 2007. Small-world anatomical networks in the human brain revealed by cortical thickness from MRI. *Cereb. Cortex* 17, 2407–2419.
- Ioannides, A.A., 2007. Dynamic functional connectivity. *Curr. Opin. Neurobiol.* 17, 161–170.
- Iturria-Medina, Y., Sotero, R.C., Canales-Rodriguez, E.J., Aleman-Gomez, Y., Melie-Garcia, L., 2008. Studying the human brain anatomical network via diffusion-weighted MRI and graph theory. *Neuroimage* 40, 1064–1076.
- Jenkins, G.M., Watts, D.G., 1968. *Spectral Analysis and Its Applications*. Holden-Day, San Francisco.
- Jiang, T., He, Y., Zang, Y., Weng, X., 2004. Modulation of functional connectivity during the resting state and the motor task. *Hum. Brain Mapp.* 22, 63–71.
- Latora, V., Marchiori, M., 2001. Efficient behaviour of small-world networks. *Phys. Rev. Lett.* 87, 198701.
- Latora, V., Marchiori, M., 2003. Economic small-world behaviour in weighted networks. *Eur. Phys. J. B* 32, 249–263.
- Ledberg, A., Akerman, S., Poland, P.F., 1998. Estimation of the probabilities of 3D clusters in functional brain images. *Neuroimage* 8, 113–128.
- Lewis, G.M., Baldassarre, A., Committeri, G., Romanina, G.L., Corbetta, M., 2009. Learning sculpts the spontaneous activity of the resting human brain. *Proc. Natl. Acad. Sci. U. S. A.* 106, 17558–17563.
- Liu, Y.J., Gao, J.H., Liotti, M., Pu, Y., Fox, P.T., 1999. Temporal dissociation of parallel processing in the human subcortical outputs. *Nature* 400, 364–367.
- Lowe, M.J., Mock, B.J., Sorenson, J.A., 1998. Functional connectivity in single and multislice echoplanar imaging using resting-state fluctuations. *Neuroimage* 7, 119–132.
- Lowe, M.J., Dzemidzic, M., Lurito, J.T., Mathews, V.P., Phillips, M.D., 2000. Correlations in low-frequency BOLD fluctuations reflect cortico-cortical connections. *Neuroimage* 12, 582–587.
- Luck, D., Danion, J.M., Marrer, C., Pham, B.T., Gounot, D., Foucher, J., 2010. The right parahippocampal gyrus contributes to the formation and maintenance of bound information in working memory. *Brain Cogn.* 72, 255–263.
- Maslov, S., Sneppen, K., 2002. Specificity and stability in topology of protein networks. *Science* 296, 910–913.
- Masson, M.F., Norton, M.I., Van Horn, J.D., Wegner, D.M., Grafton, S.T., Macrae, C.N., 2007. Wandering minds: the default network and stimulus-independent thought. *Science* 315, 393–395.
- McKiernan, K.A., D'Angelo, B.R., Kaufman, J.N., Binder, J., 2006. Interrupting the “stream of consciousness”: an fMRI investigation. *Neuroimage* 29, 1185–1191.
- Meunier, D., Achard, S., Morcom, A., Bullmore, E.D., 2009. Age-related changes in modular organization of human brain functional networks. *Neuroimage* 44, 715–723.
- Miall, R.C., Robertson, E.M., 2006. Functional imaging: is the resting brain resting? *Curr. Biol.* 16, 998–1000.
- Micheloyannis, S., Pachou, E., Stam, C.J., Vourkas, M., Erimaki, S., Tsirka, V., 2006. Using graph theoretical analysis of multi channel EEG to evaluate the neural efficiency hypothesis. *Neurosci. Lett.* 402, 273–277.
- Milo, R., Shen-Orr, S., Itzkovitz, S., Kashtan, N., Chklovskii, D., Alon, U., 2002. Network motifs: simple building blocks of complex networks. *Science* 298, 824–827.
- Peltier, S.J., LaConte, S.M., Niyazov, D.M., Liu, J.Z., Sahgal, V., Yue, G.H., Hu, X.P., 2005. Brain research-reductions in interhemispheric motor cortex functional connectivity after muscle fatigue. *Brain Res.* 1057, 10–16.
- Price, D.J., Kennedy, H., Dehay, C., Zhou, L., Mercier, M., Jossin, Y., Goffinet, A.M., Tissir, F., Blakey, D., Molnár, Z., 2006. The development of cortical connections. *Eur. J. Neurosci.* 23, 910–920.
- Raichle, M.E., Mintun, M.A., 2006. Brain work and brain imaging. *Annu. Rev. Neurosci.* 29, 449–476.
- Raichle, M.E., Snyder, A.Z., 2007. A default mode of brain function: a brief history of an evolving idea. *Neuroimage* 37, 1083–1090.
- Raichle, M.E., Macleod, A.M., Snyder, A.Z., Powers, W.J., Gusnard, D.A., Shulman, G.L., 2001. A default mode of brain function. *Proc. Natl. Acad. Sci. U. S. A.* 98, 676–682.
- Rubinov, M., Sporns, O., 2010. Complex network measures of brain connectivity: uses and interpretations. *Neuroimage* 52, 1059–1069.
- Salvador, R., Suckling, J., Coleman, M.R., Pickard, J.D., Menon, D., Bullmore, E.D., 2005a. Neurophysiological architecture of functional magnetic resonance images of human brain. *Cereb. Cortex* 15, 1332–1342.
- Salvador, R., Suckling, J., Schwarzbauer, C., Bullmore, E.D., 2005b. Undirected graphs of frequency-dependent functional connectivity in whole brain networks. *Philos. Trans. R. Soc. Lond. B Biol. Sci.* 360, 937–946.
- Schon, K., Hasselmo, M.E., Lopresti, M.L., Tricarico, M.D., Stern, C.E., 2004. Persistence of parahippocampal representation in the absence of stimulus input enhances long-term encoding: a functional magnetic resonance imaging study of subsequent memory after a delayed match-to-sample task. *J. Neurosci.* 24, 11088–11097.
- Sporns, O., Zwi, J.D., 2004. The small world of the cerebral cortex. *Neuroinformatics* 2, 145–162.
- Sporns, O., Chialvo, D.R., Kaiser, M., Hilgetag, C.C., 2004. Organization, development and function of complex brain networks. *Trends Cogn. Sci.* 8, 418–425.
- Sporns, O., Honey, C.J., Kötter, R., 2007. Identification and classification of hubs in brain networks. *PLoS One* 2, e1049.
- Sur, M., Leamey, C.A., 2001. Development and plasticity of cortical areas and networks. *Nat. Rev. Neurosci.* 2, 251–262.
- Tambini, A., Ketz, N., Davachi, L., 2010. Enhanced brain correlations during rest are related to memory for recent experiences. *Neuron* 65, 280–290.
- Tononi, G., Edelman, G.M., Sporns, O., 1998. Complexity and coherency: integrating information in the brain. *Trends Cogn. Sci.* 2, 474–484.
- Tzourio-Mazoyer, N., Landeau, B., Papathanassiou, D., Crivello, F., Etard, O., Delcroix, N., Mazoyer, B., Joliot, M., 2002. Automated anatomical labelling of activations in SPM using a macroscopic anatomical parcellation of the MNI MRI single-subject brain. *Neuroimage* 15, 273–289.
- Van den Heuvel, M.P., Stam, C.J., Boersma, M., Hulshoff Pol, H.E., 2008. Small-world and scale-free organization of voxel-based resting-state functional connectivity in the human brain. *Neuroimage* 43, 528–539.
- Vincent, J.L., Patel, G.H., Fox, M.D., Snyder, A.Z., Baker, J.T., Van Essen, D.C., Zempel, J.M., Snyder, L.H., Corbetta, M., Raichle, M.E., 2007. Intrinsic functional architecture in the anaesthetized monkey brain. *Nature* 447, 83–86.
- Wagner, A.D., Schacter, D.L., Rotte, M., Koutstaal, W., Maril, A., Dale, A.M., Rosen, B.R., Buckner, R.L., 1998. Building memories: remembering and forgetting of verbal experiences as predicted by brain activity. *Science* 281, 1188–1191.
- Waites, A.B., Stanislavsky, A., Abbott, D.F., Jackson, G.D., 2005. Effect of prior cognitive state on resting state networks measured with functional connectivity. *Hum. Brain Mapp.* 24, 59–68.
- Wang, J., Wang, L., Zang, Y., Yang, H., Tang, H., Gong, Q., Chen, Z., Zhu, C., He, Y., 2009. Parcellation-dependent small-world brain functional networks: a resting-state fMRI study. *Hum. Brain Mapp.* 30, 1511–1523.
- Wang, L., Li, Y., Metzack, P., He, Y., Woodward, T.S., 2010. Age-related changes in topological patterns of large-scale brain functional networks during memory encoding and recognition. *Neuroimage* 50, 862–872.
- Watts, D.J., Strogatz, S.H., 1998. Collective dynamics of “small-world” networks. *Nature* 393, 440–442.
- Whitfield-Gabrieli, S., et al., 2009. Hyperactivity and hyperconnectivity of the default network in schizophrenia and in first-degree relatives of persons with schizophrenia. *Proc. Natl. Acad. Sci. U. S. A.* 106, 1279–1284.
- Xiong, J., Gao, J.H., Lancaster, J.L., Fox, P.T., 1995. Clustered pixels analysis for functional MRI activation studies of the human brain. *Hum. Brain Mapp.* 3, 287–301.
- Zeki, S., Shipp, S., 1988. The functional logic of cortical connections. *Nature* 335, 311–317.
- Zhou, H.Y., Liu, J.Y., Jing, W., Qin, Y.L., Lu, S.F., Yao, Y.Y., Zhong, N., 2010. Basic level advantage and its switching during information retrieval: an fMRI study. *Proc. The 2010 international conference on brain informatics (BI 2010)*, 6334. Springer LNLI, pp. 427–436.